ADVANCES IN ATMOSPHERIC SCIENCES, VOL. 30, NO. 1, 2013, 10–14

Comments on "Direct Radiative Forcing of Anthropogenic Aerosols over Oceans from Satellite Observation"

Hye-Ryun OH[1], Chang-Hoi HO*[1], and Yong-Sang CHOI[2]

[1]*School of Earth and Environmental Sciences, Seoul National University, Seoul, Korea*

[2]*Department of Environmental Science and Engineering, Ewha Womans University, Seoul, Korea*

(Received 2 November 2011; revised 12 August 2012)

ABSTRACT

Previous observational studies have estimated anthropogenic aerosol direct radiative forcing over oceans without due consideration of cloudy-sky aerosols. However, when interaction between clouds and aerosols located below or above the cloud level is taken into account, the aerosol direct radiative forcing is larger by as much as 5 W m^{-2} in most mid-latitude regions in the Northern Hemisphere.

Key words: cloudy-sky aerosol forcing, anthropogenic aerosol, aerosol optical depth, satellite observations

Citation: Oh, H.-R., C.-H. Ho, and Y.-S. Choi, 2013: Comments on "direct radiative forcing of anthropogenic aerosols over oceans from satellite observation". *Adv. Atmos. Sci.,* **30**(1), 10–14, doi: 10.1007/s00376-012-1218-5.

1. Introduction

Recently, Chen et al. (2011) estimated anthropogenic aerosol direct radiative forcing (ARF), defined as the perturbation of top-of-the-atmosphere radiative fluxes by anthropogenic aerosols, for the year 2005 for all sky conditions (i.e., cloudy-sky and clear-sky) within the global ocean of 60°S–60°N. To determine global ARF from the observation data, they used the Single Scanner Footprint dataset, measured from the Clouds and the Earth's Energy System (CERES), and the Moderate Resolution Imaging Spectroradiometer (MODIS) onboard the *Terra* satellite. Like many other studies regarding aerosol–cloud–radiation relationships, they assumed that aerosols in cloudy regions do not exert radiative forces that compromise observational limitations (Bellouin et al., 2005). According to this assumption, ARF for all sky conditions ($ARF_{all,1}$) can be obtained by scaling the clear-sky ARF by the fraction of clear-sky region in a given grid ($1-f$):

$$ARF_{all,1}(i,j) = ARF_{clr}(i,j) \times [1 - f(i,j)] , \qquad (1)$$

where ARF_{clr} is the averaged ARF for the clear-sky region at each latitude (i) and longitude (j). In Eq. (1), it follows that $ARF_{all,1}$ is identical to ARF_{clr} under the clear-sky condition (i.e., $f = 0$) and that $ARF_{all,1}$ is zero under the overcast condition (i.e., f=1); However, in the real atmosphere, the latter is not true.

In fact, aerosol particles interact with clouds by scattering (and/or absorption) the radiation reflected from the clouds, continually exerting appreciable radiative forces (Keil and Haywood, 2003; Chand et al., 2009). In actuality, the ARF for overcast regions is not zero at all, but rather gives the combined effects of ARF_{clr} with modification of ARF by clouds (ΔARF). For this reason, Chen et al. (2011) admitted errors that resulted from the lack of consideration of ARF in cloudy regions.

It is therefore worth questioning how the value of ARF_{all} changes when cloudy-sky aerosols are included. We addressed with question by modifying Eq. (1) used in Chen et al. (2011) from a climatological perspective by using monthly averages of satellite-retrieved radiative fluxes and clouds to avoid data sampling problems. For this purpose, we employed CERES flux data (FSW, Edition 2c) and MODIS/Terra cloud data (MOD08, collection 5) with a 1°×1° resolution for the year 2005.

As noted previously, for aerosols within fractional cloud coverage f in each 1°-grid, ARF can be expressed by ARF_{clr} plus ΔARF. Thus ARF_{all} can be determined using Eq. (2):

*Corresponding author: Chang-Hoi HO, hoch@spl.snu.ac.kr

$$\begin{aligned} \mathrm{ARF}_{\mathrm{all},2}(i,j) &= \mathrm{ARF}_{\mathrm{clr}}(i,j) \times [1 - f(i,j)] + \\ &\quad [\mathrm{ARF}_{\mathrm{clr}}(i,j) + \Delta\mathrm{ARF}(i,j)] \times f(i,j) \\ &= \mathrm{ARF}_{\mathrm{clr}}(i,j) + \\ &\quad \Delta\mathrm{ARF}(i,j) \times f(i,j)\,. \end{aligned} \tag{2}$$

In Eq. (2), the estimation of $\mathrm{ARF}_{\mathrm{all},2}$ requires calculations of $\mathrm{ARF}_{\mathrm{clr}}$ and ΔARF. To calculate $\mathrm{ARF}_{\mathrm{clr}}$, we used shortwave flux values for the pristine (i.e., without aerosol and cloud) and clear-sky (i.e., with aerosol and without cloud) conditions, which were available in the CERES/FSW data. However, the challenge was the calculation of ΔARF. Because ΔARF is not observable, we had to simulate it using a radiative transfer model. We used the Santa Barbara DISORT Atmospheric Radiative Transfer (SBDART) model (Ricchiazzi et al., 1998), the flux simulations of which showed a fairly good agreement with flight observation data (Valero et al., 2003). This scheme has been popularly used in many radiation studies. The shortwave fluxes were simulated under the equivalent spectral range (i.e., 0.3–5.0 μm) of the CERES spectrometer. The prescribed shortwave insolation in the model was scaled to be comparable with the observed value from the FSW data.

To obtain ΔARF, we first built a lookup table (LUT) to describe ΔARF–cloud–aerosol relations using SBDART. To generate the LUT, the data regarding the vertical distribution of anthropogenic aerosol were needed. These data were available from the level-2 vertical feature mask observed by the Cloud-Aerosol Lidar with Orthogonal Polarization (CALIOP), which covers the field-of-view corresponding to MODIS/CERES data. The anthropogenic aerosol levels indicate the sum of polluted continental aerosols, polluted dust, and smoke aerosols, which were classified by the CALIOP. To maintain consistency among aerosol, cloud, and shortwave flux data, we used the vertical profile for the year 2005. However, the only global aerosol profile available was from the CALIOP after April 2006. According to the annual-mean vertical profiles of anthropogenic aerosol over the global ocean from the CALIOP from 2007 to 2010, interannual variability in the aerosol profile was very small. Therefore, we used the four-year (2007–2010) mean anthropogenic aerosol profile over the global ocean observed by the CALIOP. Although it is not shown as a figure, the vertical profile indicated two maximal values in the lower troposphere below 1 km (i.e., 0.4 km and 1 km). Above 1 km altitude, aerosols gradually decreased with height. The optical depth of this aerosol profile was 0.2, which corresponded to the global average.

Notably, this aerosol vertical profile was used only to generate the LUT. The LUT was then matched with MODIS-observed grid-mean bulk properties of aerosols and clouds to determine ΔARF in each grid. In this process, therefore, regional characteristics of ΔARF were captured using regionally different aerosol and cloud properties from MODIS observations, even though a fixed vertical distribution was employed.

We then allowed various feasible single-layer overcast cloud amounts with spherical droplets and aerosol conditions such as cloud optical depth (0–20), cloud effective radius (0–30 μm), surface temperature minus cloud top temperature (0–60 K)[a], aerosol single scattering albedo (ASSA; 0.87–0.99), and aerosol asymmetry factor (AAF; 0.52–0.76). Notably, the relative altitude of cloud to aerosol was indicated by cloud-top temperature under the fixed aerosol vertical profile. In this study, a difference smaller than ∼10 K indicated a case of aerosol above the cloud layer. A few exceptional cases that were not included in the LUT were also taken into account by interpolation and/or extrapolation of ΔARF via a polynomial regression function between the values of ΔARF and cloud (or aerosol) properties in the LUT.

Reliable estimation of ΔARF should be based on regionally prevailing aerosol and cloud properties. We used MODIS observations to obtain these regional properties, and all the properties were averaged monthly before their use for matchup with the LUT. To confine our focus to "anthropogenic" aerosol optical depth ($\mathrm{AOD}_{\mathrm{anth}}$), we used the methodology of Kaufman et al. (2005), in which natural coarse-mode (marine and dust) AOD is subtracted from the total AOD. This $\mathrm{AOD}_{\mathrm{anth}}$ was used to scale the ΔARF values from the LUT based on the other properties, using a factor of the ratio of [1–exp($\mathrm{AOD}_{\mathrm{anth}}$)] to [1–exp($\mathrm{AOD}_{\mathrm{LUT}}$)] (Zhao et al., 2011). Next, ASSA and AAF were obtained using the methodology of Choi et al. (2009), in which a pair (ASSA, AAF) is retrieved for each grid using two layer ARF efficiencies (i.e., $\mathrm{ARF}_{\mathrm{clr}}$ per $\mathrm{AOD}_{\mathrm{anth}}$ at the top-of-atmosphere and at the surface) because ARF efficiency is a function of only two variables: ASSA and AAF. MODIS cloud properties used in this study were the grid-mean cloud fraction, cloud optical depth, cloud effective radius, and cloud-top temperature. Finally, MODIS surface temperature was defined as the maximum brightness temperature at 11 μm over a month for each grid.

[a] We used surface temperature minus cloud-top temperature in the LUT for comparison with MODIS thermal retrievals. Because ΔARF was not directly affected by thermal condition of clouds and the surface, this difference may have been inadequate as a control parameter of ΔARF. However, the use of cloud height or pressure had the same effect on the calculation of ΔARF because the relative altitude of cloud to aerosol is much more important in determining ΔARF than the absolute altitude of cloud.

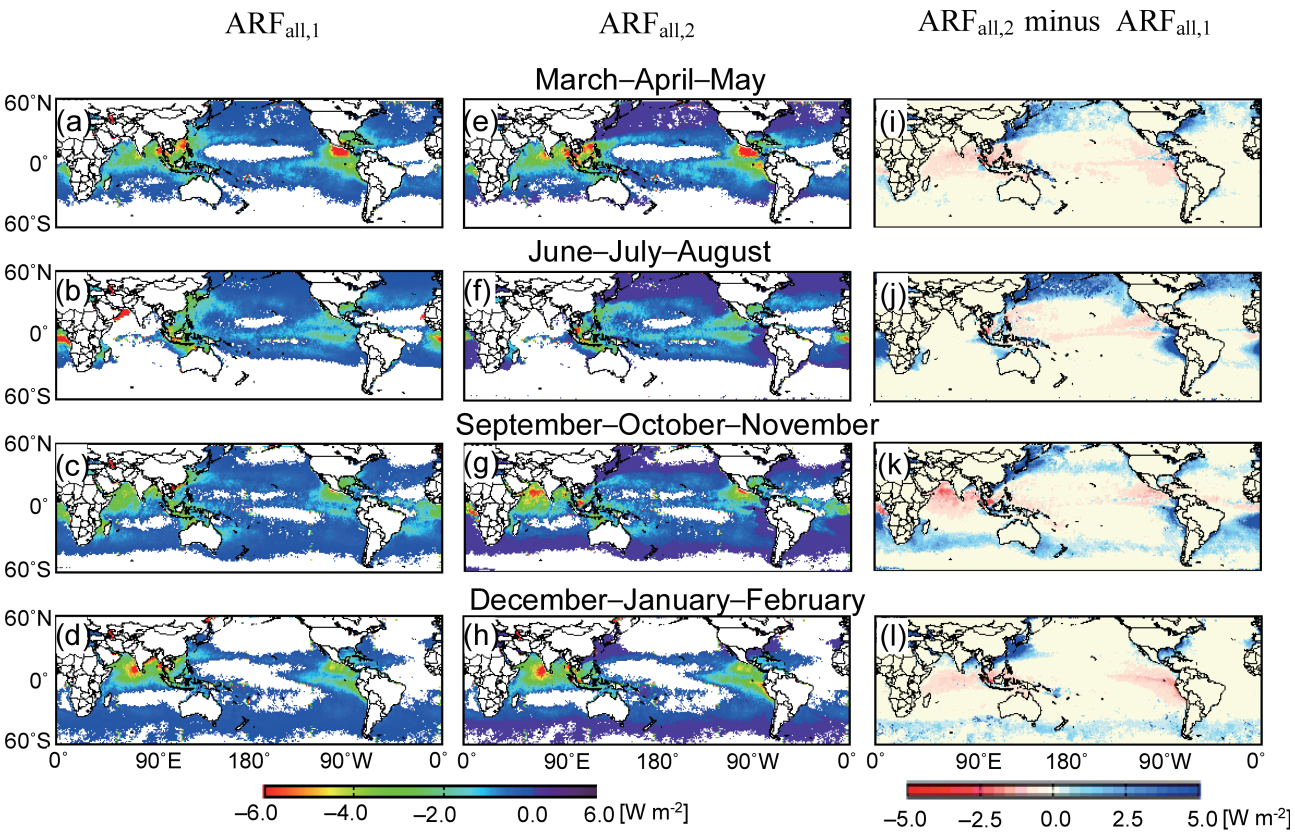

Fig. 1. Global distributions of anthropogenic aerosol radiative forcing (ARF) for all-sky by Chen et al. (2011) ($ARF_{all,1}$; a–d) and the present study ($ARF_{all,2}$; e–h) and their difference ($ARF_{all,2}$ minus $ARF_{all,1}$; i–l) for four seasons of the year 2005.

2. Distribution of aerosol direct radiative forcings

The seasonal averages of ARF_{all} [$ARF_{all,1}$ from Eq. (1) and $ARF_{all,2}$ from Eq. (2)] and their differences are presented in Fig. 1. The values of $ARF_{all,1}$ (Figs. 1a–d) mostly coincided with results from Chen et al. (2011). Relatively large cooling effects ($\leqslant -3$ W m^{-2}) occurred in the neighboring coastal seas of the Middle East, India, East Asia, Mexico, and Colombia. The annual average ± standard deviation of $ARF_{all,1}$ was -0.42 ± 0.40 W m^{-2}, which was slightly smaller than -0.34 ± 0.16 W m^{-2} (reported by Chen et al., 2011). The minor underestimation of $ARF_{all,1}$ in this study may be explained by two experimental differences. First, we used a flux for pristine condition in each grid from the CERES/FSW, whereas Chen et al. (2011) calculated it using the linear extrapolation to zero of aerosol optical depth (AOD) with respect to solar zenith angle and latitude. Second, $ARF_{all,1}$ in this study was a monthly arithmetical average of instantaneous values; however, for Chen et al. (2011) $ARF_{all,1}$ was the daily average[b]. Consequently, the methodology used in this study, though somewhat different from that of Chen et al. (2011), provided a fair comparison between $ARF_{all,1}$ and $ARF_{all,2}$.

After the influence of cloud amount on ARF in cloudy regions was considered, the spatial patterns of $ARF_{all,2}$ were plotted (Figs. 1e–h). The overall patterns of a dimming effect by anthropogenic aerosols and its seasonal variation are similar to those in Figs. 1a–d. However, the cooling effect by the aerosols was fairly diminished across the whole season, which is remarkable over the mid-latitude ocean. The annual mean ± standard deviation of $ARF_{all,2}$ was -0.12 ± 0.82 W m^{-2}. The smaller $ARF_{all,2}$ compared to $ARF_{all,1}$ shows that cloud amount, especially an optically thick and large cloud amount, can interrupt the radiation reflected back to space by aerosols and can modify the direct radiative effect of aerosols (Chand et al., 2009).

Figures 1i–l display the difference between $ARF_{all,2}$ and $ARF_{all,1}$, which indicates cloud impact on ARF_{all}. Notably, the sign of $ARF_{all,2}$ minus $ARF_{all,1}$ was pos-

[b]Daily average is a 24-h mean value by applying diurnal variation of shortwave flux assuming constant aerosol optical properties.

itive over the whole ocean because of cloud influence, which blocked out the scattering by anthropogenic aerosols. The annual mean ± standard deviation of $ARF_{all,2}$ minus $ARF_{all,1}$ was 0.53±0.63 W m^{-2}. The difference was small ($\leqslant$0.2 W m^{-2}) in low latitudes and large (>2 W m^{-2}) in mid-latitudes, particularly during summer in the Northern Hemisphere. This result implies that cloud effect on $ARF_{all,2}$ is more significant over mid-latitudes than over low latitudes.

3. Discussion and summary

Chen et al. (2011) concluded that the annual average ± standard deviation of $ARF_{all,1}$ was −0.34±0.16 W m^{-2} over the ocean between 60°S and 60°N. However, the $ARF_{all,1}$ proposed by Chen et al. (2011) may not have provided a complete explanation of the direct effect of aerosols in all sky conditions because they overlooked the influence of anthropogenic aerosols for cloudy regions. Although this simplified assumption is commonly used in aerosol–cloud–radiation relationships, it may cause uncertainty in ARF_{all}. Therefore, this study reproduced $ARF_{all,1}$ using a slightly different method from Chen et al. (2011). We additionally calculated $ARF_{all,2}$ using the same method, except we added a new consideration of the cloud impact on ARF for cloudy regions. The annual mean of $ARF_{all,2}$ minus $ARF_{all,1}$ was 0.53±0.63 W m^{-2} over the global ocean, indicating the influence of clouds that suppress scattering by anthropogenic aerosols. Particularly, $ARF_{all,2}$ minus $ARF_{all,1}$ was >2 W m^{-2} over the oceanic areas such as East Asia and the eastern United States due to a large cloud amount and cloud optical depth, which led to positive $ARF_{all,2}$ values.

There may also be a discrepancy between shortwave fluxes from RTM and from CERES. To compare RTM data with CERES-based ARF_{clr} employed in this study, we first simulated ARF_{clr} shortwave fluxes for pristine and clear conditions with respect to each latitude and solar zenith angle. In clear conditions, the shortwave flux was determined using preestimated AOD_{anth}, ASSA, and AAF given in each 1°×1° grid. The results show that the spatial pattern of RTM-based ARF_{clr} was in good agreement with CERES-based ARF_{clr} (correlation coefficient = 0.94) overall. However, RTM-based ARF_{clr} was slightly lower, by 0.13 W m^{-2} on the average, than CERES-based ARF_{clr}, which resulted from the relatively low absorptance in the model (Valero et al., 2003). Applying RTM-based ARF_{clr} to Eqs. (1) and (2), respectively, ARFs for all sky conditions (i.e., $ARF_{all,1}$ and $ARF_{all,2}$) were then calculated. Compared with the ARFs obtained from the CERES-based ARF_{clr}, the RTM-based $ARF_{all,1}$ and $ARF_{all,2}$ had negative biases of 0.05 W m^{-2} (7.04%) and 0.01 W m^{-2} (7.69%), respectively.

Our estimates of $ARF_{all,2}$ were derived from the simplified conditions of a fixed aerosol profile and a single-layer cloud due to the insufficient observations. However, cloud effects on $ARF_{all,2}$ increased when high-level aerosols (above clouds) increased. They decreased when high-level clouds (above aerosols) increased. When the aerosols were located between two cloud layers, the cloud effect on $ARF_{all,2}$ was mostly subject to the upper-level clouds. Our simplification limited the accuracy of $ARF_{all,2}$, inducing an uncertainty of approximately ±0.1 W m^{-2} on the global average.

The present results reveal that there was a significant cloud contribution to ARF in cloudy regions with respect to seasons or regions in comparison to the approach from the Chen et al. (2011). Therefore, we suggest that cloud impact on ARF_{all} and interaction with aerosol should be properly regarded with caution for cloudy regions when evaluating and interpreting ARF_{all}.

Acknowledgements. This study was supported by the Basic Science Research Program through the National Research Foundation of Korea (NRF) funded by the Ministry of Education, Science and Technology (Grant No. 2012-0000857). This work was supported by the Korean Ministry of Environment as part of the Eco-Innovation Project.

REFERENCES

Bellouin, N., O. Boucher, J. Haywood, and M. S. Reddy, 2005: Global estimate of aerosol direct radiative forcing from satellite measurements. *Nature*, **438**, 1138–1141.

Chand, D., R. Wood, T. L. Anderson, S. K. Satheesh, and R. J. Charlson, 2009: Satellite-derived direct radiative effect of aerosols dependent on cloud cover. *Nature Geoscience*, **2**, 181–184.

Chen, L., G. Y. Shi, S. G. Qin, S. Yang, and P. Zhang, 2011: Direct radiative forcing of anthropogenic aerosols over oceans from satellite observations. *Adv. Atmos. Sci.*, **28**, 973–984, doi: 10.1007/s00376-010-9210-4.

Choi, Y. S., C. H. Ho, H. R. Oh, R. J. Park, and C. G. Song, 2009: Estimating bulk optical properties of aerosols over the western North Pacific by using MODIS and CERES measurements. *Atmos. Environ.*, **43**, 5654–5660.

Kaufman, Y. J., O. Boucher, D. Tanré, M. Chin, L. A. Remer, and T. Takemura, 2005: Aerosol anthropogenic component estimated from satellite data. *Geophys. Res. Lett.*, **32**, L17804, doi: 10.1029/2005GL023125.

Keil, A., and J. M. Haywood, 2003: Solar radiative forc-

ing by biomass burning aerosol particles during SAFARI 2000: A case study based on measured aerosol and cloud properties. *J. Geophys. Res.*, **108**, 8467, doi: 10.1029/2002JD002315.

Ricchiazzi, P., S. R. Yang, C. Gautier, and D. Sowle, 1998: SBDART: A research and teaching software tool for plane-parallel radiative transfer in the earth's atmosphere. *Bull. Amer. Meteor. Soc.*, **79**, 2101–2114.

Valero, F. P. J., and Coauthors, 2003: Absorption of solar radiation by the clear and cloudy atmosphere during the Atmospheric Radiation Measurement Enhanced Shortwave Experiments (ARESE) I and II: Observations and models. *J. Geophys. Res.*, **108**, 4016, doi: 10.1029/2001JD001384.

Zhao, T. X.-P., N. G. Loeb, I. Laszlo, and M. Zhou, 2011: Global component aerosol direct radiative effect at the top of atmosphere. *Int. J. Remote Sens.*, **32**, 633–655.